Diversity-enabled sweet spots in layered architectures and speed-accuracy trade-offs in sensorimotor control

Yorie Nakahira[a,1], **Quanying Liu**[a,1], **Terrence J. Sejnowski**[b,c,2], **John C. Doyle**[a,2]

[a]**Division of Engineering and Applied Science, California Institute of Technology, Pasadena, CA 91125, USA**
[b]**The Salk Institute for Biological Studies, La Jolla, CA, USA**
[c]**Division of Biological Sciences, University of California, San Diego, La Jolla, CA, USA**

[1]These authors contributed equally
[2]To whom correspondence should be addressed; E-mail: doyle@caltech.edu, terry@salk.edu.

Nervous systems sense, communicate, compute, and actuate movement using distributed components with trade-offs in speed, accuracy, sparsity, noise, and saturation. Nevertheless, the resulting control can achieve remarkably fast, accurate, and robust performance due to a highly effective layered control architecture. However, there is no theory explaining the effectiveness of layered control architectures that connects speed-accuracy trade-offs (SATs) in neurophysiology to the resulting SATs in sensorimotor control. In this paper, we introduce a theoretical framework that provides a synthetic perspective to explain why there exists extreme diversity across layers and within levels. This framework characterizes how the sensorimotor control SATs are constrained by the hardware SATs of neurons communicating with spikes and their sensory and muscle endpoints, in both stochastic and deterministic models. The theoretical predictions of the model are experimentally confirmed using driving experiments in which the time delays and accuracy of the control input from the wheel are varied. These results show that the appropriate diversity in the properties of neurons and muscles across layers and within levels help create systems that are *both* fast *and* accurate despite being built from components that are individually slow or inaccurate. This novel concept, which we call "diversity-enabled sweet spots" (DESSs), explains the ubiquity of heterogeneity in the sizes of axons within a nerve as well the resulting superior performance of sensorimotor control.

Human sensorimotor control can achieve extremely robust performance in complex, uncertain environments, despite being implemented in systems that are distributed, sparse, quantized, delayed, and saturated. More specifically, at the hardware level, there exists a severe speed and accuracy tradeoffs. For example, achieving fast or accurate nerve signaling requires additional space and metabolic costs to build and maintain nerves, and such resource limitations impose hard SATs in nerve signaling. In contrast, at the system level, the SATs in sensorimotor control are much less severe. For example, when riding a mountain bike down a twisting, bumpy trail, though a trade-off exists between traveling fast and accurately following the trail, most human can safely stay on the trail without crashing. Such robust performance despite hardware limitations may due to highly effective layered control architectures that de-constrain the hardware constraints.

Despite the profound influence of architectures on performance, we have paid little attention to what makes an architecture effective. To understand effective layered architectures, we need to study how component constraints and trade-offs impact those on sensorimotor performance and clarify the overall system performance and limitations when different control layers act jointly. However, the hardware SATs of neural signaling (1–4) and the system SATs in sensorimotor control (5–8) have been studied separately. This is in part because there are few theoretical tools that allow us to study the hardware SATs of neural signaling (1–4) and the system SATs in sensorimotor control (5–8), or to understand the collective performance when different layers work together. In our terminology "layers" refers to different architectural components (*e.g.* planning layer, reflex layer), while "levels" refers to different levels of abstraction or composition (*e.g.* brain level vs nerve level vs molecular level, or whole muscle level vs fiber level).

We developed a mathematical theory that connects the component speed-accuracy constraints and trade-offs with those at the sensorimotor system level and provides an integrated view of a layered control systems involving planning in a high layer and reflexive reaction in a low layer. Using this theory, we show here that *diversity* between layers and within layers can be exploited to achieve *both* fast *and* accurate performance despite being implemented using slow or inaccurate hardware. We call

these synergies "diversity-enabled sweet spots" (DESSs). At the component level, this concept explains why there are extreme heterogeneities in the characteristics of neural components (Fig. 1) (2, 3, 9). At the system level, DESSs explain the benefits of extreme heterogeneities in speed and accuracy in different sensorimotor loops (10, 11).

A

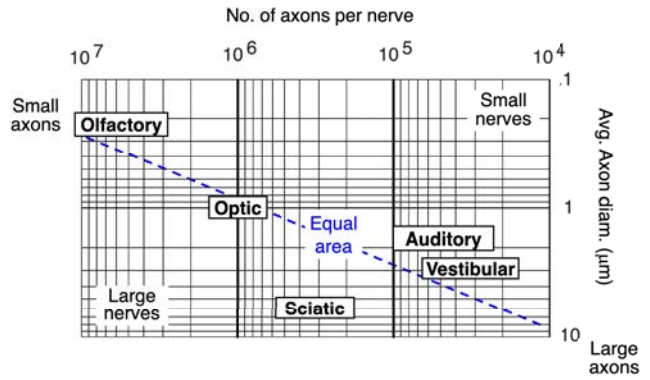

Fig. 1. Component speed-accuracy trade-offs (SATs) in sensory nerves. Sizes and numbers of axons for selected nerves and the resulting SATs. The dashed line represents nerves with equal cross-sectional area, which is proportional to λ in Eq. 3. The nerves shown have similar cross-sectional areas but wildly different compositions of axon size and number, resulting in different speed and accuracy in nerve signaling (1). A myelin sheath around an axon can also increase its speed of propagation. Many nerves, such as the sciatic nerve, contain a mixture of axons with different sizes and degrees of myelination.

Basic model. An example of an effective layered control architecture is the oculomotor system that stabilizes the eye on a moving target while you are bouncing down a trail (Fig. 2A) (10, 11). Neurons in the visual cortex responding to target motion on the retina drive the actuators to pursue the target after a delay of 100 millisecond. In contrast, fast head motions are compensated by control systems in the brainstem in the millisecond range. Together, they allow you to maintain fixation on a distant moving target despite severe bumps.

In trail following (Fig. 2B), higher-level cortical control systems in the cortex and basal ganglia provide advanced warning for planning actions to avoid trees and other obstacles. This is accompanied by a fast feedback system in the spinal cord that maintains stable tracking.

To study how these control systems are coordinated, we first introduce a driving task that simulates the trail following on a display screen. In the task, the subjects have to track a reference trail or trajectory with small errors despite unseen bumps and disturbances. We define the error dynamics $x(t)$ between the actual position (*i.e.* player's position) and the desired position (*i.e.* trail's position) as follows:

$$x(t+1) = x(t) + w(t) + u(t), \qquad [1]$$

which relates the future error $x(t+1)$ with the previous error $x(t)$, the uncertainty $w(t)$ (bumps or trail changes), and the control action $u(t)$. The control action $u(t)$ is generated using the observed errors and uncertainty as follows:

$$u(t) = \mathcal{K}(x(0:t-T_u), w(0:t-T_u+T_a-1), u(0:t-1)). \qquad [2]$$

Here, $\mathcal{K}$ is a function that defines the controller, which uses sensing components (*i.e.* eyes, muscle sensors and the inner ear), communication components (*i.e.* nerves), computing components (*i.e.* the cortex in the central nervous system), and actuation components (*i.e.* eye and arm muscles). Here, $T_u = T_s + T_i$ captures in the delay in control, which can further be decomposed into the nerve signaling delay T_s and other internal delays T_i in the feedback loop. The advanced warning T_a models the fact that the rider can view its future trail T_a time steps in advance. Its specific value is determined by the rider's speed and the trail's features, and its effect can be observed from that the muscle tone changes before an expected perturbation (12, 13). The rate constraint, R, accounts for the limitations in nerve signaling.

A

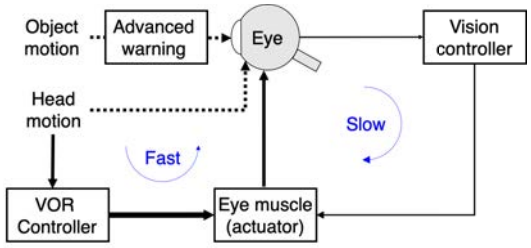

B

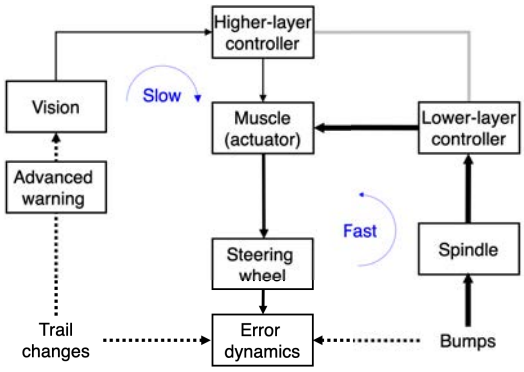

Fig. 2. Diagrams of sensorimotor control for eye tracking movements and mountain bike trail tracking. *(A)* Diagram of two major feedback loops involved in the eye movement: visual cortex feedback and vestibular-ocular reflex (VOR) feedback. Objects are tracked using the slow visual cortex feedback, while head motion is compensated for by the much faster VOR feedback. *(B)* Diagram of the basic sensorimotor control model for our experiment that simulates riding a mountain bike. Each box is designated by its function: sensing and communication (*e.g.* vision, muscle spindle sensor, vestibulo-ocular reflex), actuation (muscle), and computation (high-layer planning and tracking and low-layer reflexes and reactions). Depending on the hardware details, they may be quantized (discrete valued), have time delays, experience saturation, and be subject to noise. The trail ahead can be seen in advance, but the bumps and other disturbances are unanticipated. The line thickness indicates the relative speed of the pathway (thicker lines for faster pathways.

Hardware SATs. There exists trade-offs between neural signaling speed and accuracy arising from the fixed spatial and metabolic cost to build and maintain axons. Specifically, nerves with the same cross-sectional area can either contain many small axons or a few large axons (Fig. 1), which inevitably leads to SATs in neural signaling (1–3). The specific forms of SATs depend on how the nerves encode information (*e.g.* spike-based, rate-based, and spike-interval-based encoding). Our theory does not require any specific forms of encoding methods and the resulting hardware SATs, so for simplicity, we assume the spike-based encoding scheme in our analysis in the main text. In the spike-based encoding, information is encoded in the presence or absence of a spike within each time interval, analogous to digital packet-switching networks (14, 15). This encoding requires spikes to be generated with sufficient timing accuracy, which has been experimentally verified in many types of neurons (16, 17). To model the complex size distributions in axon bundles in a nerve, we classify axons into m distinct types, where each type corresponds to axons of identical size. We index each type by $k \in \{1, 2, \cdots, m\}$ and model type k axons as a communication channel with signaling delay T_k and signaling rate R_k (*i.e.* the total amount of information in bits that can be transmitted per unit time). It can be shown that

$$R_k = \lambda_k T_k \qquad \sum_{k=1}^{m} \lambda_k = \lambda \qquad [3]$$

where $\lambda_k \geq 0$ and $\lambda > 0$ are constants associated with the total resource (*i.e.* space available to build the axons) used by type k axons and all axons, respectively. See the supplementary information for more detail. A special case of Eq. 3 is that all axons have the same size. In such case, we can model the axon bundles as a single communication channel with signaling delay $T_s = T_1 = T_2 = \cdots = T_m$ and signaling rate $R = \sum_{k=1}^{m} R_k$ satisfying

$$R = \lambda T_s. \qquad [4]$$

For other types of encoding, we refer interested readers to the supplementary information.

System SATs imposed by hardware SATs. The hardware SATs imposes the SATs in sensorimotor control. To study its impact, we consider the motivating example of riding a mountain bike, which is simulated by our driving game experiments (see Materials and Methods). The error between the actual and desired positions evolves according to Eq. 57. The feedback loop Eq. 2 can transmit R bits of information with delay $T := T_u - T_a = T_s + T_i - T_a$ from sensing (of the disturbance) to actuation. We characterize the worst-case error and the average-case error in sensorimotor control. The worst-case error is more applicable to risk-averse sensorimotor behaviors, such as riding a mountain bike on a cliff/trail, in which staying on the cliff is necessary for survival even in the presence of the worst possible uncertainty (18–21). The average-case error is more applicable to risk-neutral sensorimotor behaviors, such as riding a mountain bike across a broad field, in which there is no fatal risk of leaving the field (1).

The worst-case error $\max_{\|w\|_\infty \leq 1} \|x\|_\infty$ is lower-bounded by

$$\max(0, T+1) + \left(2^R - 1\right)^{-1}. \qquad [5]$$

In this case, the mean squared error $\lim_{n\to\infty}(1/n)\sum_{t=1}^{n} \mathbb{E}[x(t)^2]$ is lower-bounded by

$$\max(0, T+1) + \left(2^{2R} - 1\right)^{-1}. \qquad [6]$$

The proof of Eq. 5, Eq. 6 and more general results are given in the supplementary information. The performance bounds in both settings (Eq. 5–6) are qualitatively similar: both bounds decompose into two terms. The shared first term, $\max(0, T+1)$ (denote as the delay error), is only a function of the total delay and thus can be considered as the cost due to delay. The second terms, $(2^R - 1)^{-1}$ and $(2^{2R} - 1)^{-1}$ (denote as the rate error), are only functions of the signaling rate and can be considered as the cost due to rate limits.

Since the validity of our framework does not require the hardware SATs to have any specific form, we next use the SAT in spike-based encoding to demonstrate how the SATs at the component level impact the SATs at the system level. By combining the hardware SATs in Eq. 4 and the system SATs in Eq. 5 and Eq. 6, we can predict the influence of the neural signaling constraints on sensorimotor control, shown in Fig. 3A. Increasing the delay in the feedback loop increased the delay errors, while increasing rate led to a large decrease in the rate errors. The errors for the trials with both added delay and added quantization was approximately the sum of the errors for the trials with the delay and the quantization added separately, as predicted by the model. Thus, the delays can cause small disturbances to escalate into larger errors (22), and increasing the data rate dramatically reduces errors in the context of control.

Furthermore, the minimum reaching time or the minimum error is achieved when the deleterious effects of the nerve signaling delay and inaccuracy are both controlled within a moderate range. Conversely, the nerve composition that either maximize the speed or accuracy in nerve signaling results in suboptimal performance. This observation suggests that the analysis of neural design principle and its capability for information transfer should be studied together with sensorimotor control.

Experimental test of model predictions. The predictions of the model were confirmed experimentally with driving game experiments (see Materials and Methods for more details). The subjects played the driving game under three different conditions: with added delay, with added

Parameter	Description
$x(t)$	Error at time step t
$\mathcal{K}$	Controller
$T_s \geq 0$	Signaling delay
$T_a \geq 0$	Advanced warning
$T_i \geq 0$	Internal delay
$T = T_s + T_i - T_a$	Total delay
R	signaling rate (bits per unit time)
λ	Cost associated with the resource use

Table 1. Parameters in the basic model.

quantization, or with added delay and quantization. Their trajectories were measured and the errors were analyzed and shown in Fig. 3B.

Similar to the theoretical prediction, constrained by the hardware SAT, Eq. 4, the optimal performance is achieved at a sweet spot of intermediate levels with added delay and quantization rate. Conversely, minimizing either the added delay or the rate independently leads to suboptimal performance.

Layered control systems. In this section we will examine two biological control systems that combine slow advanced planning with fast reflexive reaction.

Visual tracking of a moving object. The above results can be used to study the effectiveness of the layered control architecture used in the oculomotor system. Visual tracking of a moving object is done through two major feedback loops: a VOR feedback loop that compensates for head motion and a visual feedback loop through the visual cortex that tracks a moving object (Fig. 2A). From a control perspective, an important difference of the two loops is their levels of advanced warning. VOR feedback reacts after head moves, while the visual environment is highly correlated over time and thus are also predictable. We refer to the regime of VOR feedback *delayed reaction*, in which the net delay $T_i - T_a$ is positive, and the uncertainty $w(t)$ becomes accessible to the controller *after* $w(t)$ affects the error dynamics. We refer to the regime of visual feedback *advanced planning*, in which $T_a - T_i \geq 0$, and the uncertainty $w(t)$ becomes accessible to the controller *before* $w(t)$ affects the error dynamics. These two regimes are qualitatively different in their optimal choice of T_s and R for achieving optimal robust performance, as shown in Fig. 4A and summarized below.

(i) Delayed reaction: When the net delay $T_i - T_a > 0$ is large, the total error can be much larger than the size of the uncertainty $\|w\|_\infty$ and goes to infinity as $T_i \to \infty$. This large error amplification is consistent with the all-too-familiar observation that even a small bump on a trail can cause a cyclist to lose control of the bike and crash. As T_i increases, the delay error increasingly dominates the total error. Since the delay error largely contributes to the total error, the total error is minimized when T_s is set

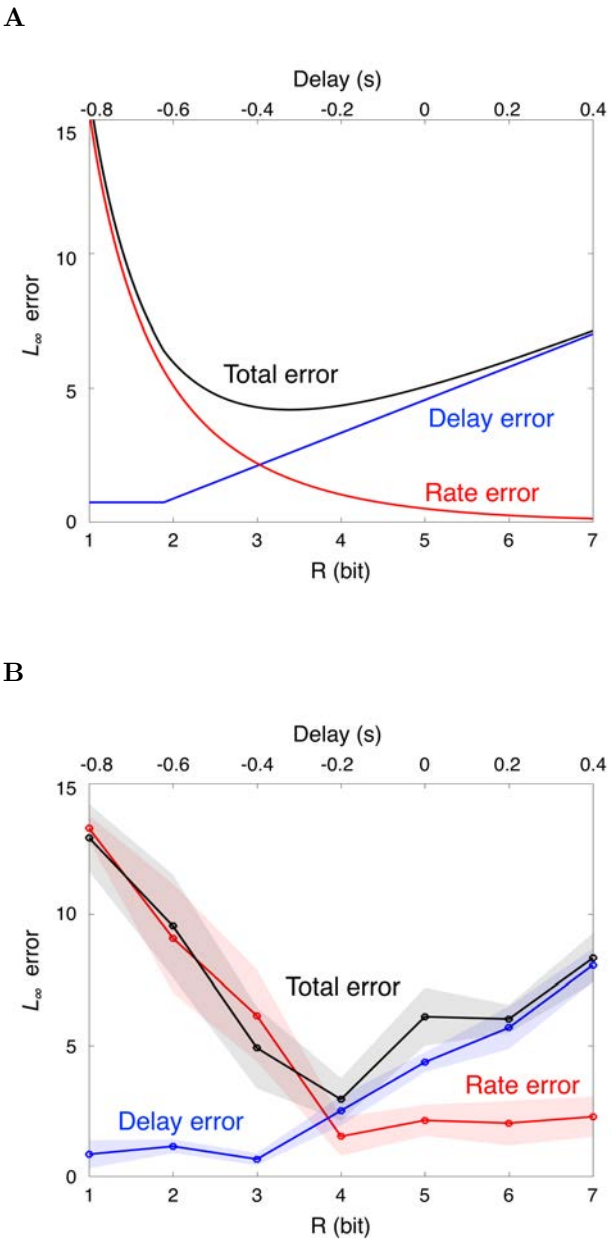

Fig. 3. Theoretical and experimental system SATs in sensorimotor control *(A)* Theoretical SATs in the tracking (driving) task. The delay error (blue), rate error (red), and the total error (black) in Eq. 5 are shown with varying hardware SAT $T = (R - 5)/20$. *(B)* Empirical SATs in the tracking (driving) task averaged over 4 subjects. The error under added delay (blue), the error under added quantization (red); and the error under added delayed and quantization (black) are shown. In the last case, the added delay T and quantization rate R satisfy $T = (R-5)/20$. The shadowed area indicates the standard error across subjects.

to be small in return for small R. Therefore, a feedback loop in this regime performs better when it is built from a few large axons. Interestingly, the flat optimal delay/rate within the delayed reaction regime suggests that optimal performance can be achieved using one type of nerve composition for a broad range of advanced warnings. This property is beneficial because the net delay (defined from advanced warning) differs across different sensorimotor

tasks.

(ii) Advanced planning: When the net warning $T_a - T_i > 0$ is large, the total error approaches zero as $R \to \infty$. This large disturbance attenuation is consistent with the observation that a cyclist can avoid obstacles given enough time to plan a response, *e.g.* route a path around them or brace against their impact. Given sufficiently large advanced warning T_a, the rate error increasingly dominates the total error because the growth in T_s incurs no additional delay error. Since the rate error contributes largely to the total error, the total error is minimized when the signaling rate R is set to be large at the expense of large signaling delay T_s. Therefore, a feedback loop in this regime performs better when it is built from many small axons.

This prediction is qualitatively consistent with the anatomy of the human oculomotor system (Fig. 1). The vestibular nerve, which transmits motion information from the inner ear to the vestibular nucleus in the brainstem, has $20,000$ axons with mean diameter $3\,\mu m$ and coefficient of variation $0.4\,\mu m$. In contrast, the optic nerve carrying visual signals from the retina has approximately 1 million axons with mean diameter $0.6\,\mu m$ and coefficient of variation $0.5\,\mu m$, significantly smaller but more numerous and with greater variability (1). As a consequence, feedback from visual processing is slower (approximately 100 ms delay) but more accurate than the VOR feedback (approximately 10 ms delay) (23).

This diversity in control performance can also be observed in two simple tests: moving one's hand left and right across the visual field with increasing frequency while holding the head still (Test 1); and shaking the head back and forth (in a 'no' pattern) at increasing frequency while holding the hand still (Test 2). In Test 1, the hand starts to blur at around 1-2 Hertz due to delays in tracking. In Test 2, blurring due to the inability to compensate for fast head motion occurs at a much higher frequency. This difference illustrates that the visual cortex feedback responsible for Test 1 (object tracking) has lower levels of tolerable delays than the VOR feedback responsible for Test 2 (head motion compensation). However, though slower, the visual cortex feedback is more accurate than the VOR feedback. This is illustrated by the fact that standing on one leg with closed eyes is more difficult than with eyes open.

Riding a mountain bike. The study of oculomotor system reveals that nerves with appropriate diversity allows the visual systems to react to head motion quickly and collect accurate visual information. This kind of DESS is ubiquitous in sensorimotor control. For example, consider the DESSs in the control architectures used for riding a mountain bike. The task of riding a mountain bike was simulated using the driving game experiments. The control system associated with the task is shown in Fig. 2B.

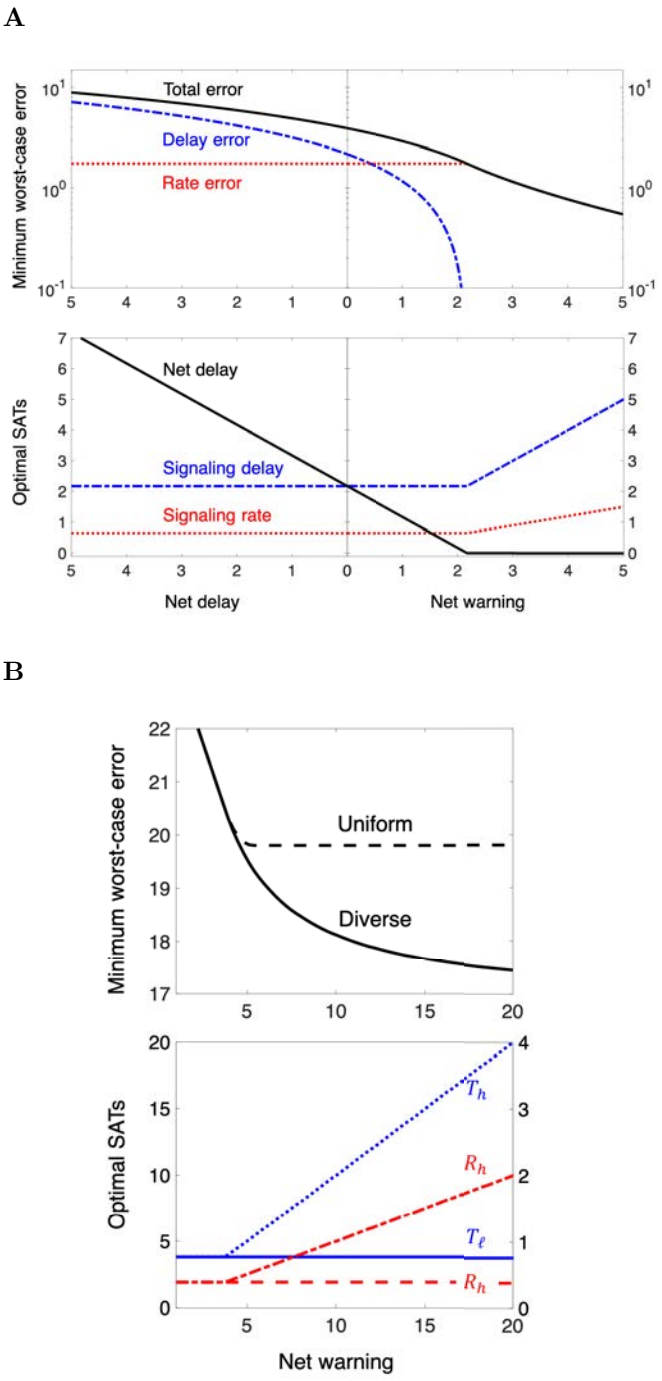

Fig. 4. Delayed reaction vs. advanced planning *(A)* Comparison between the regime of advanced warning and that of delayed reaction. The top figure shows the minimum total error Eq. 5 (the delay error plus the rate error) given a fixed resource level λ. The bottom figure shows the optimal signaling delay T_s, total delay $T = T_s + T_i - T_a$, and rate $R = \lambda T_s$ for varying net delay $T_i - T_a$. In both figures, the horizontal axes denote the net delay $T_i - T_a \geq 0$ or the net warning $T_a - T_i \geq 0$. *(B)* The benefit of diversity between planning and reflex layers. The top figure shows the minimum error Eq. 99 for the case when the high-layer and low-layer controllers are allowed to have *diverse* signaling delays and rates and otherwise (*i.e.* $R_\ell = R_h$ and $T_\ell = T_h$). We term the former the diverse case and the latter the uniform case. The high-layer controller can better exploit the advanced warning to minimize errors in the diverse case than in the uniform case. The bottom figure shows the resulting optimal delays and rates for the diverse case. System parameters are set to be $R_\ell = 0.1T_s$, $R_h = 0.1T_h$, and $T_i = 10$.

Specifically, the error dynamics is given by

$$x(t+1) = x(t) + u_L(t) + u_H(t) + w(t) + r(t - T_a), \quad [7]$$

where $w(t)$ captures the disturbance due to trail bumps, and $r(t)$ captures the curvature of the desired trajectory. There are two major feedback loops that act to control the error $x(t)$: a reflex feedback loop that compensates for bumps, and a planning feedback loop that determines which trajectory to follow. These feedback controllers can be written as

$$\begin{aligned} u_h(t) &= H(r(0 : t - T_h + T_a), u(0 : t-1)) \\ u_\ell(t) &= L(w(0 : t - T_\ell - T_c), u(0 : t-1)) \\ u(t) &= Q_m(Q_\ell(u_\ell(0 : t)), Q_h(u_h(0 : t))). \end{aligned} \quad [8]$$

Here H is a high-layer planner and L is a low-layer disturbance compensator. The object position $r(t)$ is accessible to the controller with advanced warning T_a, which models its predictability.

The accuracy constraint of each controller is modeled by quantizers Q_ℓ, Q_h with signaling rates R_ℓ, R_h. The commands from both controllers are put into action by the cyclist's muscles, the accuracy of which is modeled by a quantizer Q_m with signaling rate R_m. Let $\bar{R}_\ell$ and $\bar{R}_h$ be defined by $\bar{T}_\ell := T_\ell + T_c$, $\bar{R}_\ell := \min(R_\ell, R_m)$, $\bar{T}_h := T_h - T_a$, and $\bar{R}_h := \min(R_h, R_m)$. In the driving task with sufficiently large advanced warning T_a, the state-deviation $\sup_{\|w\|_\infty \le \epsilon, \|r\|_\infty \le 1} \|x\|_\infty$ achievable by the controller Eq. 8 is lower-bounded by

$$\left\{ \bar{T}_\ell + \frac{1}{2^{\bar{R}_\ell} - 1} \right\} \epsilon + \frac{1}{2^{R_h} - 1}. \quad [9]$$

Interestingly, the overall error lower-bound is the sum of the error in the high-layer and the error in the low-layer. Intuitively, this property holds because the feedback control system Eq. 7-8 can be decomposed into two independent sub-systems, each involving H or L (See the section of separability of subsystems and the Supplementary Information for more detail).

Fig. 4B compares the performance of the control system with diverse layers or with uniform layers. It suggests that diversity between layers allow the overall system to exploit advanced warning in order to reduce errors. Specifically, having diverse layers improves the system SATs, which in turn allows for a reduced total error.

Separability of subsystems. To confirm that the sum of the errors from each loop adds up to be the total error, we designed three types of driving experiments: with bump only, with trail changes only, and with both bump and trail changes. Our experimental results are shown in Fig. 5. The error from the combined bump and trail session positively correlated with the sum of the errors from the bump only session and the trail only session (Pearson correlation, correlation coefficient = 0.57), and they showed no significant difference. The results suggest

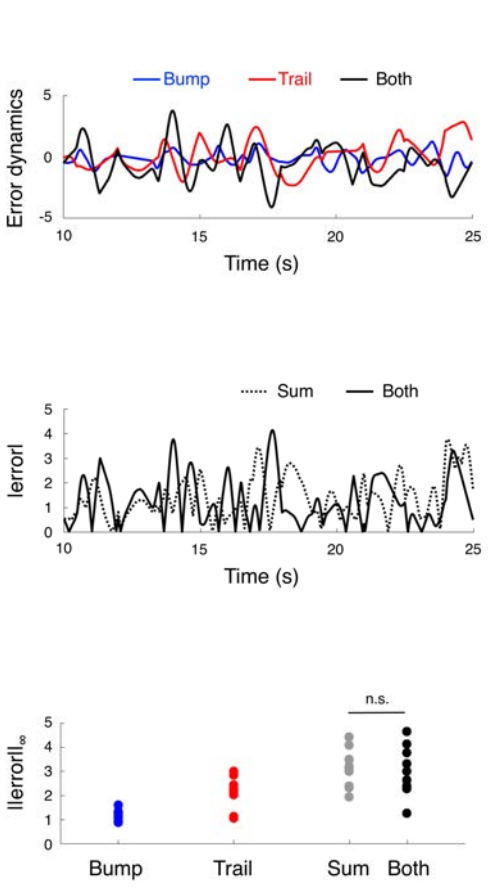

Fig. 5. Errors when subjects perform the bump and/or trail tasks (A) Error dynamics from a task with only bump, a task with only trail, and a task with both; (B) Absolute values of the sum of errors from the first two tasks and the error from the last task; (C) Worst-case error for the three tasks and the sum of errors from the first two cases. Each dot denotes the worst-case error in an interval of 2 seconds.

that the two feedback loops can be analyzed separately, which is also consistent with Eq. 99.*

The separation of Eq. 99 into the individual errors caused by two subsystems allows us to use the preceding insight to study the layered control architecture used in the driving tasks. The reflex feedback typically operates in the regime of delayed reaction, as reflexes often sense bumps only after the bike has hit them. The planning feedback typically works in the regime of advanced planning, as the bike's trajectory can often be seen in advance. Similar to the case of the oculomotor system, the reflex feedback has better performance when it is designed to have a small signaling delay at the expense of a low signaling rate; in contrast, the planning feedback is constructed to have a large signaling rate at the expense of a large signaling delay (25, 26).

DESSs between layers. The above two case studies suggest that diversity between different layers helps achieve *both* fast *and* accurate sensorimotor control despite the

*Such separation of different feedback loops is common in many processes, *e.g.* (24).

A

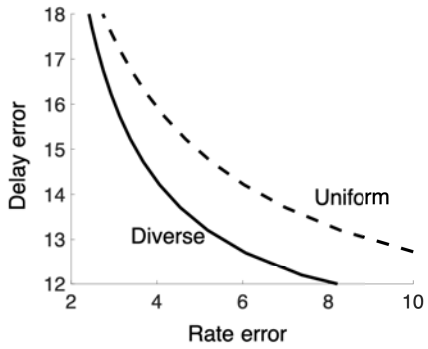

B

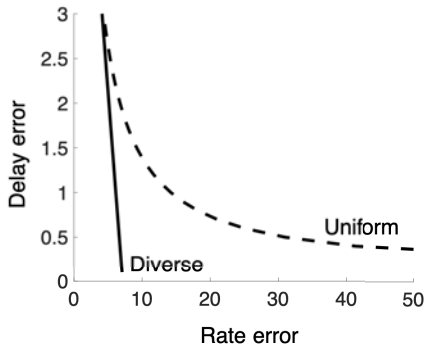

Fig. 6. Examples of diversity-enabled sweet spots *(A)* The benefit of diversity between layers. We set $\lambda = 0.1$ and $T_i - T_a = 0$. The delay error and rate error are defined to be the sum of the delay errors in both the high-layer and low-layer and that of the rate errors in both layers, respectively. *(B)* The benefit of diversity within a level. The figure shows that diversity in axons enables the system to achieve better SAT in sensorimotor control. We use $m = 1$ for uniform nerves and $m = 2$ for diverse nerves, and we set $\lambda = 0.1$ and $T_i - T_a = 0$. We define the delay error to be T_1 in Eq. 12, *i.e.* the errors caused before the first spike arrives, and the rate error to be the remaining terms.

slowness or inaccuracy of individual layers. This benefit is illustrated in Fig. 6A. The hardware SAT imposes system tradeoffs between minimizing the delay errors or rate errors in sensorimotor control. However, the diverse case has a less severe SAT by using a slow but accurate high-layer to reduce the rate cost and an inaccurate but fast low-layer to reduce the delay cost. We name this *diversity-enabled sweet spots* (DESSs), *i.e.* diversity helps de-constrain the hardware SATs to achieve a sweet spot in the tradeoff space between speed and accuracy.

DESSs within a layer. Analogously, diversity within a layer also helps deconstrain the component SATs. To see it, we extend our framework to capture the effects of diversity in neural composition on performance. For the system Eq. 57 and axons of diverse sizes, the state-deviation $\max_{\|w\|_\infty \le 1} \|x\|_\infty$ is lower-bounded by

$$\sum_{h=1}^{\infty} \frac{1}{2^{\mathcal{R}(h)}}. \qquad [10]$$

where the function $\mathcal{R} : \mathbb{Z}_+ \to \mathbb{R}_+$ is defined to be

$$\mathcal{R}(h) := \sum_{k=1}^{m} \max\{0, h - T_k - T_i + T_a\} R_i. \qquad [11]$$

See the Supplementary Information for more detail. For example, at $m = 2$, the error lower bound is reduced to

$$T_1 + \frac{1 - 2^{-R_1(T_2 - T_1)}}{2^{R_1} - 1} + \frac{1}{2^{R_1(T_2 - T_1)}} \frac{1}{2^{R_1 + R_2} - 1}. \qquad [12]$$

Fig. 6B compares the system SATs when the control is implemented using axons of diverse size or uniform size. Similarly, systems with diverse axons have an improved SAT compared with systems with uniform axons, implying that diversity in nerve composition can boost the speed and accuracy of the system. This phenomenon is another example of DESSs. It also suggests the benefit of having diversity in axon sizes, particularly in optic, vestibular, and sciatic nerves (2, 3).

Discussion. Nerves have limited signaling speed and accuracy, and there exist trade-offs between the two (Fig. 1). To understand how such nerves can collectively achieve remarkably robust sensorimotor control, we developed a theoretical framework that characterizes how hardware SATs in nerve signaling translates to system SATs in sensorimotor control (Fig. 3). The results suggest that a highly effective layered control architecture with the proper diversity enables fast and accurate performance to be achieved using slow or inaccurate hardware (Fig. 6). For instance, the vestibulo-ocular system (Fig. 2) has an inaccurate but fast layer that performs negative feedback control to stabilize images on the retina against rapid head movements and a slower but accurate layer to perform smooth pursuit for tracking slowly moving visual objects (10, 11). These two layers jointly create a virtual eye controller that is both fast and accurate. More generally, DESSs can be observed in the layered architectures used in many types of sensorimotor control tasks and decision making (27). DESS can also explain why the size principle for the recruitment of motor units produces an optimal trade-off between speed and accuracy, which is needed to explain Fitts' Law in reaching (28, 29). So, the DESSs theory may reveal a more general design principle for distributed control in brains and inspire the design of large-scale technological systems.

Our results suggest several interesting research directions. The first is to more thoroughly explore the parameter space for the experimental tasks in a larger number of subjects. The driving game could be diagnostic for patients with motor disabilities. The second is to compare the optimal control and communication structures with the actual sensorimotor control system. For example, the optimal controllers resemble predictive coding, in the sense that they transfer prediction errors from sensors to actuators in order to make the most of the available

signaling rate. This predictive coding may be the reason why there is massive feedback from higher cortical areas back to V1 (30). The third is to adapt the theory to other behaviors with speed-accuracy tradeoffs (see (31) and references therein), including cognitive and voluntary tasks by adding additional layers in the feedback loops. Further refining and clarifying how hardware SATs impact the system SATs in such tasks will illuminate fundamental limits, trade-offs, and the effectiveness of central nervous system architectures in a quantitative manner.

Moreover, the DESSs theory can be widely applied to other complex systems, from the biomolecular control in a single cell to advanced technological systems like the Internet of Things. The goal is to better understand how to achieve accurate vs. fast systems using slow or inaccurate layers built from the inexpensive hardware. Below, we list some examples of systems that could benefit from the DESS framework, and envision a broader use of layered architecture and DESSs in both biological and engineering systems.

Motor Learning. There are many other sensorimotor learning tasks that exploit DESSs. Consider learning how to shoot a basketball. Most beginners use a deliberative process at a high cognitive layer to predict the trajectory and carefully execute the shot. With more experience, parts of the process are automatized by reflexes in lower layers. The higher planning layer, which is expensive and extensively used initially, is slower but can flexibly adapt to new tasks. In contrast, the lower reactive layers, which gradually take over control as the learning proceeds, can only perform a limited set actions but are fast. This process of sensorimotor learning is essentially distributing the control process across several layers with different speed and accuracy so that the task can be performed fast and accurately.

Immune response. Our immune system also exploits DESS to perform fast and targeted immune responses. There is a tradeoff between reacting to an infection quickly versus producing a response that is targeted toward a specific type of infection. When infection occurs, the immune system produces a fast general response, followed by a sequence of slower but more targeted responses (32, 33). The combination of fast general response and slow targeted responses improves the overall effectiveness of the immune response, thereby increasing the probability of survival.

Power system. DESSs can also be found in power systems. A power system combines a planning layer that decides the best operating levels of the plants with a disturbance-rejection layer that makes local adjustments to maintain stability. The planning layer typically solves an optimal power flow problem to determine the best operating levels of the plants that meet demands with minimal operation cost (34). The disturbance-rejection layer uses various control processes such as frequency control to continuously monitor the demands and control the frequency at each generating station (35). The decision to set the operating level of the whole system is slow due to delays in data aggregation, communication, and computation. In contrast, local controllers can respond faster, but they cannot change the operating level of the whole system. Combining these two allows the power system to exhibit both speed and flexibility.

Cloud versus edge computing. DESSs can also be observed in the Internet of Things applications, which use cloud and edge computers to decide on control actions. The capacity of the cloud computer can be used to perform extensive computation to find optimal decisions, which are slowed by the time needed for aggregating sensor information and communicating control decisions across the network (36). In contrast, edge computers are able to respond to their nearby local sensors quickly, but may only be able to take suboptimal control actions on a limited set of tasks in the absence of global information (37). Although each controller has its own limitations, an appropriate combination of these two layers of control can achieve fast and efficient performance.

Rate-based encoding is a slower alternative hardware SAT to spike-based encoding. The information in neuron action potential spikes can be encoded in many different ways (14, 16, 17, 23). Eq. 3 characterizes the neural signaling SATs in spike-based encoding. Interestingly, rate-based-encoding (38) also leads to similar SATs:

$$R_k = \frac{\lambda_k}{2} T_k \qquad \sum_{k=1}^{m} \lambda_k = \lambda. \qquad [13]$$

where λ is previously given in Eq. 3 (see the supplementary information for the detailed definition) is proportional to the spatial and metabolic cost to build and maintain the nerves. Interestingly, spike-based encoding and rate-based encoding have qualitatively similar SATs: given a fixed resource (space and metabolic cost to build and maintain nerves), the achievable signaling rate is roughly proportional to delay. However, the spike-based encoding has a better SAT than the SAT of rate-based encoding given a fixed resource level λ. This property can be seen from the fact that achieving the same rate R_i requires the signaling delay of R_i/λ in spike-based encoding and $2R_i/\lambda$ in rate-based encoding. The derivation for Eq. 13 can be found in the Supplementary Information.

Actuator saturation: An alternative system SAT. Our framework can flexibly accommodate different assumptions and models. One such extension is actuator saturation. In the deterministic framework, we model the sensorimotor control system using the error dynamics $x(t+1) = ax(t) + u(t) + w(t)$, where $\{w(t)\}$ is a sequence of bounded variables satisfying $\|w\|_\infty \leq 1$. If the system in Eq. 57 is stable, *i.e.* $|a| < 1$, then there is no trade-off between the minimum error that can be attained with

the minimal saturation level

$$\sup_{\|w\|_\infty \le 1} \|u\|_\infty = \left(|a^T| + \frac{|a^T|}{2^R - |a|}\right)\left(1 - \frac{1}{2^R}\right) =: \ell \quad [14]$$

In contrast, when the system is marginally stable or unstable, *i.e.* $|a| \ge 1$, the minimal state-deviation subject to $\|u(t)\|_\infty \le \ell$ is given by

$$\begin{cases} \sum_{i=1}^{T} |a^{i-1}| + |a^T| \frac{1}{2^R - |a|} & \text{if } \ell \le |a| \frac{2^R - 1}{2^R - |a|} \\ \sum_{i=1}^{T} |a^{i-1}| + |a^T| \frac{1 - \ell}{1 - |a|} & \text{otherwise.} \end{cases} \quad [15]$$

In the stochastic framework, we model the sensorimotor control system with the same error dynamics, but let $\{w(t)\}$ to be a sequence of *i.i.d.* random variables with mean 0 and variance 1. In addition to the signaling rate constraints, we impose the following saturation constraints on the average control power

$$\lim_{n\to\infty} \frac{1}{n} \sum_{t=1}^{n} \mathbb{E}[u(t)^2] \le \ell. \quad [16]$$

We adapt the results of control under information constraints (39–42) to explicitly characterize the impact of information constraints, delay, and actuator saturation. Specifically, let $P : \mathbb{R}_+ \to \mathbb{R}_+$ and $G : \mathbb{R}_+ \to \mathbb{R}_+$ be functions given by $P(\lambda) = \{1 - \lambda + a^2\lambda + \sqrt{4\lambda + (a^2\lambda - \lambda + 1)^2}\}/2$, $G(\lambda) = a^2 P^3 (a^2\Lambda + a^{2(T+1)} - \Lambda)/(P^2 + 2\lambda P + \lambda^2 + \lambda a^2 P^2)$, where $\Lambda = a^{2(T+1)}/(2^{2R} - a^2)$. When $\ell < G(0)$, we define λ^* to be the strictly positive scalar that satisfies[†]

$$G(\lambda^*) = \ell. \quad [17]$$

When $\ell \ge G(0)$, we set $\lambda^* = 0$. Given such λ^*, we define the scalars P^* and G^* to be $P^* = P(\lambda^*)$ and $G^* = G(\lambda^*)$,[1] respectively. Then, the state-deviation $\inf \lim_{n\to\infty} \frac{1}{n} \sum_{t=1}^{n} \mathbb{E}[x(t)^2]$ is lower bounded by

$$\left\{\sum_{i=1}^{T} a^{2(i-1)}\right\} + P^* a^{2(T+1)} + \frac{a^{2(T+1)}(P^* a^2 - P^* + 1)}{2^{2R} - a^2},$$

which can be achieved with the control effort $\lim_{n\to\infty}(1/n)\sum_{t=1}^{n} \mathbb{E}[u(t)^2] = G(\lambda^*)$. When $a = 1$ and $\ell = \infty$, we have $\lambda^* = 0$, $P(\lambda^*) = 1$, $G(\lambda^*) = 1$, and therefore

$$\lim_{T\to\infty} \frac{1}{T} \sum_{t=1}^{T} \mathbb{E}[x(t)^2] \ge T + \frac{1}{2^{2R} - 1} \quad [18]$$

Interestingly, although the control effort generally depends on the signaling rate, for $a = 1$, $\lim_{n\to\infty}(1/n)\sum_{t=1}^{n} \mathbb{E}[u(t)^2] = 1$ does not have such a dependency.

[†] Observe that $G(\lambda) \ge 0$ by construction. In addition, the solution of Eq. 17 is unique.

Materials and Methods. We developed a platform for a driving game that simulates riding a mountain bike (43). The platform is inexpensive and easy to implement. The code and manual to build the platform are available at https://github.com/Doyle-Lab/WheelCon. During the experiment, the subject looked at a PC monitor and steered a wheel to follow the desired trajectory. The trajectory had a constant velocity for each segment but abruptly switched between right and left segments. The console for the driving task is shown in Fig. 7.

To test the effects of delay or quantization, we conducted experiments in which the subjects played the driving game with added delay and quantization inbetween the wheel (control input) and the actual position (target of control). The additional delays were $T = -0.8, -0.6, \cdots, 0.4$ seconds. Here, negative delays were realized by adding advance warning in the vision input, while the positive delays were implemented by adding an external delay in actuation. The rate of the quantizer was set to be $R = 1, 2, \cdots, 7$ bits per unit time. When both the delay and the quantizer are inserted, the added delay T and the quantizer rate R satisfy $T = (R - 5)/20$. Each set of parameters lasted for 30 seconds before switching to a new set of parameters. The first 10 seconds of each 30 second trial were not used to measure the performance in order to eliminate switching and learning effects. Before each experiment, subjects were trained until their performance stabilized.

We conducted experiments with four participants. Plots of L_∞ norm error between the road (the desired position) and the current position of the player are shown in Fig. 3B. Additionally, we tested SATs for the stochastic settings, shown in Fig. S2 in the supplementary material.

To study how different layers multiplex, we conducted the driving game experiments with bump, trail changes, or both. When both were used, the bump disturbance and trail changes were generated independently. The bumps were generated by pushing the steering wheel at a constant torque for 0.5 second. The trial was generated with the angle $\theta \in \{10°, 20°, \ldots, 80°\}$ and alternated between left and right with exponentially distributed time, such that the participants cannot anticipate the trial trajectory without advanced warning in vision. The results of this experiment, shown in Fig. 5, confirm that the the reflex and planning layers multiplex well.

ACKNOWLEDGMENTS. This research was supported by National Science Foundation (NCS-FO 1735004 and 1735003) and the Swartz Foundation. Q.L. was supported by a Boswell fellowship and a FWO postdoctoral fellowship (12P6719NLV)

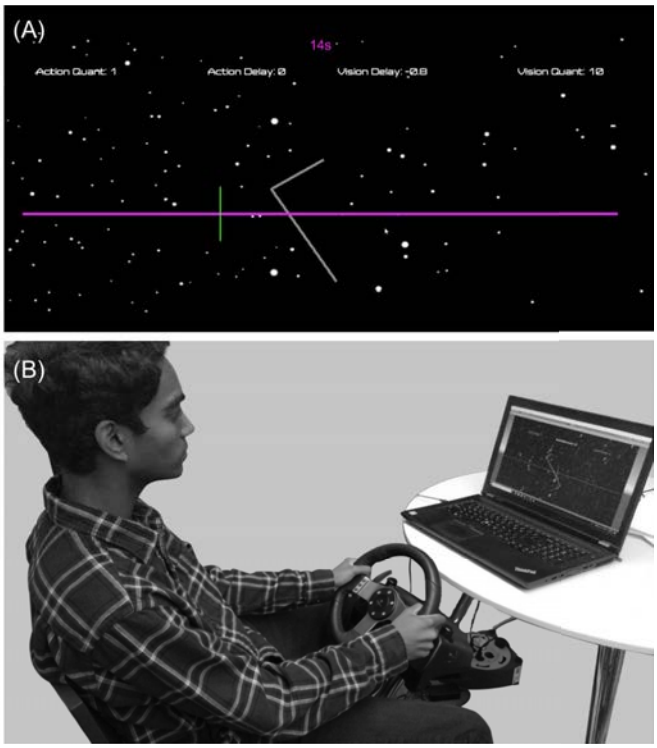

Fig. 7. Video monitor interface for the driving task. *(A)* Players see a winding trail scrolling down the screen at a fixed speed, and thus with a fixed look-ahead time T, both of which can be varied widely. The player aims to minimize the error between the desired trajectory and their trues screen position using a gaming steering wheel. *(B)* Bumps are added using a motor torque in the wheel. Experiments can be done with just bumps or trails, or both together, and with varying trail speed and/or T, and with additional quantization and/or delay in the map from wheel position to player screen position.

Supplementary materials

Overview

In this supplementary document, we develop the basic theory needed to derive the results presented in the main text. To this end, we apply the tools from robust control theory, which characterizes the performance of a feedback system using its input-output relation (44, 45). The emerged expressions are reminiscent of the bounds in a stochastic system derived using information theoretic arguments (40, 41, 46) but they can be derived using the time-domain arguments that rely on linear algebra only. In section 1, we derive the fundamental limits in system performance as a function of the delay and data rate in the deterministic worst-case setting. The resulting optimal controllers have an interesting analogy to predictive coding, which is commonly observed in the visual system and other sensorimotor processes (47). In section 2, we consider an alternative setting of stochastic average-case and derive the fundamental limits in system performance. In section 3, we derive the neural signaling SAT when axons encode information in spike rate. In section 4, we present some additional experimental results.

Notations. We use lower case letters to denote sequences, *i.e.* $x = \{x(0), x(1), x(2), \dots\}$, and $x(t_1 : t_2)$ to denote a truncated sequence of x from t_1 to t_2, *i.e.* $x(t_1 : t_2) = \{x(t_1), x(t_1 + 1), \cdots, x(t_2)\}$. The ∞-norm of a sequence x is defined as $\|x\|_\infty := \sup_t |x(t)|$, and the 1-norm of a sequence x is defined as $\|x\|_1 = \sum_{t=0}^{\infty} |x(t)|$. The mutual information between two random variables x, y with the probability density function P is defined using $I(x; y) = \mathbb{E}\left[\log(P(x, y)/P(x)P(y))\right]$. We use Q to denote a quantizer that approximates a continuous domain with a finite set of values. The quantizer is defined by 2^R intervals partitioned by $\{p[\ell]\}$ and their respective representation points $\{c[\ell]\}$ such that

$$Q(x) = \begin{cases} c[1] & x \in [p[0], p[1]) \\ c[2] & x \in [p[1], p[2]) \\ \vdots & \\ c[2^R] & x \in \left[p[2^R - 1], p[2^R]\right), \end{cases} \tag{19}$$

where R is referred to as its data rate. We denote $\bar{Q}_{R,\Psi}$ to be a uniform quantizer with data rate R and domain $[-\Psi, \Psi]$, which partitions its domain into 2^R intervals with equal lengths and maps the input from each interval to the middle point of that interval.

1. Deterministic setting with worst-case performance

A. Systems with delay. We consider the error dynamics

$$x(t + 1) = ax(t) + w(t) + u(t) \tag{20}$$

where $x(t) \in \mathbb{R}$ is the error state, $u(t) \in \mathbb{R}$ is the control action, $w(t) \in \mathbb{R}$ is the disturbance, and $a \in \mathbb{R}$ defines the error dynamics evolution. We assume zero initial condition, *i.e.* $x(0) = 0$. The controller $\mathcal{K}$ generates the control action $u(t)$ using the full information on the histories of the error, disturbance, and control input with delay $T_u \geq 0$, *i.e.*

$$u(t) = \mathcal{K}(x(0 : t - T_u), w(0 : t - T_u - 1), u(0 : t + T_u - 1)) \tag{21}$$

The sensorimotor control in risk-aware setting motivates the use of L_1 optimal control, and as such, our goal is to solve the following robust control problem:

$$\inf_{\mathcal{K}} \sup_{\|w\|_\infty \leq 1} \|x\|_\infty \tag{22}$$

subject to Eq. 20 and Eq. 21. This problem admits a simple and intuitive solution. In particular, the optimal cost is given by

$$\inf_{\mathcal{K}} \sup_{\|w\|_\infty \leq 1} \|x\|_\infty = \sum_{i=0}^{T_u} |a^i|. \tag{23}$$

This optimal cost is achieved by the control policy

$$u(t) = -a^{T_u+1} w(t - T_u - 1). \tag{24}$$

To prove Eq. 23 and Eq. 24, we first first derive a lower bound for the optimal cost, and we then find a controller that achieves the lower bound. The lower bound is obtained by noticing that the delay T_u in the control loop introduces an initial uncontrollable window in the closed loop response of the system. So we have

$$\begin{aligned} \max_{\|w\|_\infty \leq 1} \|x\|_\infty &\geq \max_{\|w\|_\infty \leq 1} |x(T_u + 1)| \\ &\geq \max_{\|w\|_\infty \leq 1} |a^{T_u} w(0) + a^{T_u - 1} w(1) + \cdots + w(T_u)| \\ &= \textstyle\sum_{i=0}^{T_u} |a^i| \end{aligned}$$

This lower bound can also be realized by the control policy Eq. 24, which yields the following closed loop behavior

$$x(t+1) = a^{T_u} w(t - T_u) + a^{T_u - 1} w(t - T_u + 1) + \cdots + w(t).$$

From Eq. A, we observe that the worst-case disturbance is

$$\begin{aligned} &w(t - T_u) = \operatorname{sign}(a^{T_u}) \\ &w(t - T_u + 1) = \operatorname{sign}(a^{T_u - 1}) \\ &\vdots \\ &w(t) = 1 \end{aligned}$$

which attains the optimal cost in Eq. 23.

B. Systems with quantization. Quantization is the process of converting a continuous signal to a discrete one. It can arise in many biological systems where sensing, computation, and actuation components are not co-located. We consider the error dynamics Eq. 20 and a quantized controller

$$u(t) = \mathcal{K}(x(0:t), w(0:t-1), u(0:t-1)) \tag{25}$$

where $x(t) \in \mathbb{R}$ is the system error, $u(t) \in \mathbb{R}$ is the control action, and $w(t) \in \mathbb{R}$ is the disturbance. We also assume zero initial condition, *i.e.* $x(0) = 0$. The desired control action $u(t)$ is generated by the controller $\mathcal{K}$ using full information on the histories of error, disturbance, and control input, but the feedback loop can only transmit R bits of information per unit time. In all of what follows, we assume that the data rate is above the minimum stabilizing rate, *i.e.* $R > \log_2 |a|$ (48). This problem also admits an analytic formula

$$\inf_{\mathcal{K}} \sup_{\|w\|_\infty \le 1} \|x\|_\infty = \frac{|a|}{2^R - |a|} + 1, \tag{26}$$

which can be attained by the control policy

$$u(t) = \bar{Q}_{R,\Psi}(-ax(t)) \tag{27}$$

where $\Psi = 2^R |a| / (2^R - |a|)$, and the map $Q_{R,\Psi}$ is defined to be a uniform quantizer of rate R on domain $[-\Psi, \Psi]$.

Similarly, Eq. 26 and Eq. 27 can be proved by first lower-bounding the optimal cost and then find a controller that achieves the bound. A lower bound can be obtained using the problem of estimating $w(\tau)$ at time t:

$$H(t,\tau) = \inf_{Q} \sup_{|w(\tau)| \le 1} |w(\tau) - \hat{w}(\tau)| \tag{28}$$

$$\text{s.t.} \quad \hat{w}(\tau) = Q(w(\tau)) \tag{29}$$

$$Q \text{ is a quantizer with data rate } (t-\tau)R. \tag{30}$$

Because $w(\tau)$ can take any values in the interval $[-1, 1]$, and the output of $Q(w(\tau))$ can take at most $2^{(t-\tau)R}$ discrete values, the estimation error is lower-bounded by $H(t,\tau) \ge 2^{-(t-\tau)R}$. On the other hand, the above lower bound can also be attained using a uniform quantizer on domain $[-1, 1]$. It then follows that

$$H(t,\tau) = \begin{cases} 2^{-(t-\tau)R} & t \ge \tau + 1 \\ 1 & t < \tau + 1. \end{cases} \tag{31}$$

The problem $H(t,\tau)$ can be used to lower-bound the value of $|x(t+1)|$. The error can be decomposed into terms due to past disturbance and a term due to past control action:

$$x(t+1) = a^t w(0) + a^{t-1} w(1) + \cdots + w(t) + U'(t), \tag{32}$$

where $U(t) = \sum_{\tau=0}^{t} a^\tau u(t-\tau)$. We define an auxiliary error x' and its control action U' as follows:

$$x'(t+1) = a^t w(0) + a^{t-1} w(1) + \cdots + w(t) + U(t) \tag{33}$$

$$U'(t) = -(a^t \hat{w}(0) + a^{t-1} \hat{w}(1) + \cdots + \hat{w}(t)), \tag{34}$$

where $\hat{w}(\tau)$ is the optimal solution of the estimation problem $H(t,\tau)$. The worst-case absolute value of $x'(t+1)$ can be easily computed as

$$\sup_{\|w\|_\infty \le 1} |x'(t+1)| \tag{35}$$

$$= \sup_{\|w\|_\infty \le 1} |a^t(w(0)-\hat{w}(0)) + a^{t-1}(w(1)-\hat{w}(1)) + \cdots + (w(t)-\hat{w}(t))| \tag{36}$$

$$= \sup_{\|w\|_\infty \le 1} |a^t(w(0)-\hat{w}(0))| + |a^{t-1}(w(1)-\hat{w}(1))| + \cdots + |w(t)-\hat{w}(t)| \tag{37}$$

$$= |a^t|H(t,0) + |a^{t-1}|H(t,1) + \cdots + H(t,t) \tag{38}$$

$$= \frac{1-(|a|/2^R)^{t+1}}{1-|a|/2^R} \tag{39}$$

This value monotonically increases as time t grows. Under the assumption $R > \log_2 |a|$, we have

$$\lim_{t\to\infty} \frac{1-(a/2^R)^t}{1-(a/2^R)} = \frac{2^R}{2^R-|a|}, \tag{40}$$

where the convergence of the infinite series is due to the assumption on minimum stabilizing data rate, *i.e.* $|a|/2^R < 1$. Meanwhile, the disturbance $w(\tau)$ can take any values from $[-1,1]$, and at most $2^{(t-\tau)R}$ bits of information can be used to transmit the information on $w(\tau)$ during the time interval $[\tau,t]$. Therefore, the control action $U(t)$ for $x(t+1)$ cannot perform better than $U'(t)$ for $x'(t+1)$, *i.e.*

$$\sup_{\|w\|_\infty \le 1} |x(t+1)| \ge \sup_{\|w\|_\infty \le 1} |x'(t+1)|. \tag{41}$$

Combining Eq. 35–Eq. 41, we obtain the following lower bound on the achievable cost:

$$\sup_{\|w\|_\infty \le 1} \|x\|_\infty \ge \lim_{t\to\infty} \sup_{\|w\|_\infty \le 1} |x(t+1)| \ge \lim_{t\to\infty} \sup_{\|w\|_\infty \le 1} |x'(t+1)| = \frac{2^R}{2^R-|a|}. \tag{42}$$

Next, we show that the control policy Eq. 27 achieves the optimal cost Eq. 26. Let $u^*(t)$ be the input to the quantizer, and $x_q(t+1) = \bar{Q}_{R,\Psi}(u^*(t)) - u(t)$ be the quantization error. Observe that $x(t) = w(t-1) + x_q(t)$. Using mathematical induction, it can be shown that there exists a control and communication policy that achieves

$$\sup_{\|w\|_\infty \le 1} \|x_q\|_\infty \le \frac{|a|}{2^R-|a|}. \tag{43}$$

Condition in Eq. 43 holds at time $t=0$. Now we assume that condition in Eq. 43 holds at time t. It then follows that

$$|u^*(t)| = |-ax(t)| = |-a(x_q(t)+w(t-1))| \le \frac{2^R|a|}{2^R-|a|} = \Psi. \tag{44}$$

Since the quantizer output $\bar{Q}_{R,\Psi}(u(t))$ can take at most 2^R discrete values, the value of $x_q(t+1)$ can be bounded by

$$|x_q(t+1)| = |\bar{Q}_{R,\Psi}(u^*(t)) - u^*(t)| \tag{45}$$

$$\le 2^{-R}\Psi \tag{46}$$

$$= \frac{|a|}{2^R-|a|}. \tag{47}$$

Thus, condition Eq. 43 also holds at time $t+1$, and this finishes the proof of Eq. 43. Combining Eq. 42 with Eq. 43 yields

$$\sup_{\|w\|_\infty \le 1} \|x\|_\infty = \sup_{\|w\|_\infty \le 1} \|x_q + w\|_\infty \le \frac{|a|}{2^R-|a|} + 1.$$

C. Basic systems with delay and quantization: the reaching tasks. The above analysis tool can be used to study the fundamental limits in a reaching task and derive a formula similar to Fitts' law (5). In a reaching task, the goal is to move a hand, eye etc. to a target of distance D as quickly and accurately as possible. This setting can be recovered by the error dynamics Eq. 20, where the error $x(t) \in \mathbb{R}$ is defined as the distance between the target and desired position with initial condition $x(0) = 0$, the control action $u(t) \in \mathbb{R}$ captures the control effort for reaching, and the disturbance $w(t) \in \mathbb{R}$ satisfies $w(t) = w\delta(t) \in \mathbb{R}$ and $|w| \le D$ ($\delta(t)$ is a Kronecker delta function). The control action is generated by

$$u(t) = \mathcal{K}(x(0:t-T_u), w(0:t-T_u-1), u(0:t-1)), \tag{48}$$

which can transmit the full information on the histories of the error, disturbance, and control input, R bits per unit time with a delay of T_u. The reaching time T_r can be formally defined as

$$T_r = \inf\{t : |x(t)| \le W/2 \text{ for any } |w| \le D\} \tag{49}$$

The worst case reaching time is lower-bounded by

$$\max_{|w|\le D} T_r \ge T_u + R^{-1}\log_2\left(\frac{2D}{W}\right). \tag{50}$$

To show Eq. 50, we define the problem of estimating $w(0)$ at time t as follows, similar to the case in section B:

$$H(t,0) = \inf_{Q} \sup_{|w(0)|\le D} |w(0) - \hat{w}(0)| \tag{51}$$

$$\text{s.t.} \quad \hat{w}(0) = Q(w(0)) \tag{52}$$

$$Q \text{ is a quantizer with data rate } (t - T_u)R. \tag{53}$$

The value of $H(t,0)$ can be computed to be

$$H(t,0) = \frac{1}{2^{(t-T_u)R}} D. \tag{54}$$

The minimum worst-case reaching time is lower-bounded by

$$\max_{|w|\le D} T_r \ge \min\{t : H(t,0) \le W/2\} \tag{55}$$

$$\ge T_u + R^{-1}\log_2\left(\frac{2D}{W}\right). \tag{56}$$

For more detail and its implications, we refer interested readers to our companion paper (28), which studies Fitts' law from the perspective of diversity sweet spot (DESSs).

D. Basic systems with delay and quantization: the driving tasks. We consider the system with delayed and quantized control:

$$\begin{aligned} x(t+1) &= ax(t) + w(t - T_a) + u(t) \\ u(t) &= \mathcal{K}(x(0:t-T_u), w(0:t-T_u-1), u(0:t-1)) \end{aligned} \tag{57}$$

where $x(t) \in \mathbb{R}$ is the system error, $u(t) \in \mathbb{R}$ is the control action, and $w(t) \in \mathbb{R}$ is the disturbance. We also assume zero initial condition, *i.e.* $x(0) = 0$. The controller $\mathcal{K}$ receives advanced warning on disturbance T_a ahead of time. The feedback loop involving $\mathcal{K}$ can transmit at most R bits of information about the full information on the histories of the error, disturbance, and control input, with a delay of T_u. We assume that the data rate R is minimum stabilizing, *i.e.* $R > \log_2|a|$. This problem also admits a simple and intuitive solution. In particular, the optimal cost is given by

$$\min_{\mathcal{K}} \max_{\|w\|_\infty \le 1} \|x\|_\infty = \begin{cases} \displaystyle\sum_{i=0}^{T} |a^i| + |a^{T+1}| \left(2^R - |a|\right)^{-1} & \text{if } T > 0 \\ \left(2^R - |a|\right)^{-1} & \text{if } T \le 0, \end{cases} \tag{58}$$

where $T := T_u - T_a$ is the net delay from the disturbance to the control action. The optimal cost only depends on $T_u - T_a$ but not individual values of T_u and T_a because systems with constant $T_u - T_a = T$ can all be reduced to systems with either $(T_a, T_u) = (-T, 0)$ for $T \le 0$ or $(T_a, T_u) = (0, T)$ for $T > 0$. Therefore, the proof for optimal cost and optimal control policy in the case of $T < 0$ is given in Eq. 27. On the other hand, the optimal control policy for $T > 0$ is

$$\begin{aligned} x_q(t) &= u(t-1) - u^*(t-1) \\ u^*(t) &= -a^{T+1} w(t - T - 1) - a x_q(t) \\ u(t) &= \bar{Q}_{R,\Psi}(u^*(t)), \end{aligned} \tag{59}$$

where $\Psi = 2^R|a^{T+1}|/(2^R - |a|)$.

Similar to previous cases, we prove Eq. 58 and Eq. 59 by first deriving a lower bound of the optimal cost and then finding a controller that achieves the lower bound. To obtain the lower bound, we decompose the error $x(t)$ into the term due to delayed control $x_d(t)$ and the term due to quantized control $x_q(t)$ as follows:

$$x(t) = x_d(t) + x_q(t). \tag{60}$$

Because the information about the disturbance $w(t-T:t)$ is not available to the controller when generating the control signal $u(t)$, its effect on $x(t+1)$ cannot be controlled. It then follows that the effects of $w(t-T:t)$ on $x(t+1)$ is

$$x_d(t+1) = a^T w(t-T) + a^{T-1} w(t-T+1) + \cdots + w(t). \tag{61}$$

Given the term $x_d(t+1)$, we can then define

$$x_q(t+1) = x(t+1) - x_d(t+1), \tag{62}$$

which is a function of $w(0:t-T-1)$ and $u(0:t)$, but not $x_d(t+1)$. Here, disjoint subsets of the disturbance affect the term due to delay $x_d(t+1)$ and the term due to quantization $x_q(t+1)$, and the value of $x_d(t+1)$ is not impacted by the chosen control policy. Therefore, the optimal cost can also be decomposed into

$$\inf_{\mathcal{K}} \sup_{\|w\|_\infty \le 1} \|x\|_\infty = \sup_{\|w\|_\infty \le 1} \|x_d\|_\infty + \inf_{\mathcal{K}} \sup_{\|w\|_\infty \le 1} \|x_q\|_\infty, \tag{63}$$

where the infima on both sides are subject to the system dynamics Eq. 57. From Eq. 61, the first term satisfies

$$\sup_{\|w\|_\infty \le 1} \|x_d\|_\infty = \sum_{i=0}^{T} |a^i|. \tag{64}$$

We will show below that the second term satisfies

$$\inf_{\mathcal{K}} \sup_{\|w\|_\infty \le 1} \|x_q\|_\infty \ge \frac{|a^T|}{2^R - |a|}. \tag{65}$$

Similar to the case in section B, we define the problem of estimating $w(0)$ at time t as follows:

$$\begin{aligned} H(t,\tau) = \inf_{Q} \quad & \sup_{|w(\tau)| \le 1} |w(\tau) - \hat{w}(\tau)| \\ \text{s.t.} \quad & \hat{w}(\tau) = Q(w(\tau)) \\ & Q \text{ is a quantizer with data rate } (t-T-\tau)R. \end{aligned} \tag{66}$$

Now we use the estimation problem $H(t,\tau)$ to lower-bound the value of $|x_q(t+1)|$. The term $x_q(t+1)$ can also be decomposed into

$$x_q(t+1) = a^t w(0) + a^{t-1} w(1) + \cdots + a^{T+1} w(t-T-1) + U(t), \tag{67}$$

where $U(t) = \sum_{\tau=0}^{t-T} a^\tau u(t-T-\tau)$. We define an auxiliary error x' and its control action U' as follows:

$$x'_q(t+1) = a^t w(0) + a^{t-1} w(1) + \cdots + a^{T+1} w(t-T-1) + U(t) \tag{68}$$

$$U'(t) = -(a^t \hat{w}(0) + a^{t-1} \hat{w}(1) + \cdots + a^{T+1} \hat{w}(t-T-1)), \tag{69}$$

where $\hat{w}(\tau)$ is the optimal solution of the estimation problem $H(t,\tau)$. The worst-case absolute value of $x'_q(t+1)$ can be bounded by

$$\begin{aligned} & \sup_{\|w\|_\infty \le 1} |x'_q(t+1)| \\ &= \sup_{\|w\|_\infty \le 1} |a^t(w(0) - \hat{w}(0))| + |a^{t-1}(w(1) - \hat{w}(1))| + \cdots + |a^{T+1}(w(t-T-1) - \hat{w}(t-T-1))| && [70] \\ &= |a^t| H(t,0) + |a^{t-1}| H(t,1) + \cdots + |a^{T+1}| H(t, t-T-1) && [71] \\ &= \frac{|a^{T+1}|}{2^R} \frac{1 - (|a|/2^R)^{t-T}}{1 - (|a|/2^R)} && [72] \end{aligned}$$

From the same argument with section B, the control action $U(t)$ for $x_q(t+1)$ cannot perform better than $U'(t)$ for $x'_q(t+1)$, *i.e.*

$$\sup_{\|w\|_\infty \le 1} |x_q(t+1)| \ge \sup_{\|w\|_\infty \le 1} |x'_q(t+1)| \tag{73}$$

The lower-bound on $\sup_{\|w\|_\infty \le 1} |x'_q(t+1)|$ monotonically increases as time t grows. Taking $t \to \infty$, we obtain that

$$\begin{aligned} \sup_{\|w\|_\infty \le 1} \|x_q\|_\infty &\ge \lim_{t\to\infty} \sup_{\|w\|_\infty \le 1} |x_q(t+1)| && [74] \\ &\ge \lim_{t\to\infty} \sup_{\|w\|_\infty \le 1} |x'_q(t+1)| && [75] \\ &\ge \frac{|a^{T+1}|}{2^R - |a|}. && [76] \end{aligned}$$

where the infinite series in Eq. 76 converges because the data rate is assumed to be minimum stabilizing, *i.e.* $|a|/2^R < 1$. Combining Eq. 64 and Eq. 65, we obtain the following lower bound on the optimal cost

$$\|x\|_\infty \geq \sum_{i=1}^{T} |a^{i-1}| + \frac{|a^{T+1}|}{2^R - |a|}. \tag{77}$$

Next, we find a control policy that achieves the lower bound Eq. 58. We follow the same procedure with section B to show that the controller Eq. 59 achieves

$$\sup_{\|w\|_\infty \leq 1} |x_q(t)| \leq \frac{|a^{T+1}|}{2^R - |a|}. \tag{78}$$

Condition in Eq. 78 holds for $t = 0$. Now we assume that condition in Eq. 78 holds for time t. It then follows that

$$|u^*(t-T)| = |-ax_q(t) - a^{T+1}w(t-T-1)| \leq |a^{T+1}| \left(1 + \frac{|a|}{2^R - |a|}\right) = \Psi. \tag{79}$$

Therefore, the value of $x_q(t+1)$ is bounded by

$$|x_q(t+1)| = \frac{|a^{T+1}|}{2^R - |a|}. \tag{80}$$

Thus, condition Eq. 78 holds at time $t+1$. Combining Eq. 64 and Eq. 78 yields

$$\max_{\|w\|_\infty \leq 1} \|x\|_\infty \leq \sum_{i=0}^{T} |a^i| + \frac{|a^{T+1}|}{2^R - |a|}.$$

The optimal controller Eq. 59 works as follows: it first uses the disturbance information to predict future errors; then, it compares the error prediction with the actual value; finally, it sends out only the error signals. The optimal controllers for a similar setting, generated from the System Level Synthesis (SLS) method, also involve a procedure to estimate $w(t)$ and $x(t)$ (involving $\hat{w}(t)$ and $\hat{x}(t)$ in (49)), which are then used to compute the control actions. Interestingly, both resemble predictive coding—a ubiquitous process appearing across sensing, cognition, and control systems (47). Predictive coding is a strategy to use available communication capability efficiently: a system uses an internal model to predict the future signal so that only the error between the prediction and the actual signal needs to be transmitted.

E. Refined control system with loops involving diverse speed and accuracy. We consider the system dynamics Eq. 20 with the feedback controller $\mathcal{K}$ of the form

$$[s_1(t), s_2(t), \cdots, s_m(t)] = K_t(x(0:t), w(0:t+T_a), s(0:t-1)) \tag{81}$$

$$u(t) = \sum_{k=1}^{m} Q_{t,i}(s_i(t - T_k - T_c)), \tag{82}$$

where $x(t) \in \mathbb{R}$ is the error, $w(t) \in \mathbb{R}$ is the disturbance, $u(t) \in \mathbb{R}$ is the control action. We assume that the disturbance is ∞-norm bounded and, without loss of generality, $\|w\|_\infty \leq 1$.

Recall from Eq. 66 that $H(t, \tau)$ is defined to be the problem of estimating $w(\tau)$ at time t. Its worst-case estimation error can be computed by

$$H(t, \tau) = \frac{1}{2^{\mathcal{R}(h)}} \tag{83}$$

where $\mathcal{R} : \mathbb{Z}_+ \to \mathbb{R}_+$ is defined to be

$$\mathcal{R}(h) := \sum_{k=1}^{m} \max\{0, h - T_k - T_c + T_a\} R_k. \tag{84}$$

Adapting the same procedure with section D, we obtain that the worst-case error is bounded by

$$\min_{\mathcal{K}} \max_{\|w\|_\infty \leq 1} \|x\|_\infty \geq \sum_{h=1}^{\infty} |a^{h-1}| \frac{1}{2^{\mathcal{R}(h)}}, \tag{85}$$

yielding Eq. 10 in the main text.

Next, we construct a control policy that achieves the equality of Eq. 85. To begin, without loss of generality, we assume that $T_1 < T_2 < \cdots < T_m$ and $R_k > 0$ for $k \in \{1, 2, \cdots, m\}$. We define the following terms recursively.

$$\begin{aligned}
&\hat{w}(t, k, \tau) = 0 \text{ for } t - \tau \le T_1 \\
&\hat{w}(t, k+1|\tau) = \bar{Q}_{R_{k+1}, \ell_{t-\tau,k+1}}(w(\tau) - \hat{w}(t, k|\tau)) + \hat{w}(t, k|\tau) \text{ for } k \in \{1, 2, \cdots, p-1\} \text{ and } T_1 < t - \tau \le T_{p+1} \\
&\hat{w}(t+1, 1|\tau) = \bar{Q}_{R_1, \ell_{t-\tau+1,1}}(w(\tau) - \hat{w}(t, k|\tau)) + \hat{w}(t, m|\tau) \text{ for } k = p
\end{aligned} \tag{86}$$

where ℓ is recursively defined by

$$\ell_{T_1,1} = 1 \tag{87}$$

$$\ell_{t-\tau,k+1} = \ell_{t-\tau,k}/2^{-R_k} \text{ for } k \in \{1, 2, \cdots, p\} \qquad \text{if } T_1 < t - \tau \le T_{p+1} \tag{88}$$

$$\ell_{t-\tau+1,1} = \ell_{t-\tau,k}/2^{-R_k} \text{ for } k = p \qquad \text{if } T_1 < t - \tau \le T_{p+1} \tag{89}$$

We define the scaled estimation errors to be

$$e(t, k|\tau) = a^{t-\tau}(w(t) - \hat{w}(t, k|\tau)) \tag{90}$$

Let $Q_{t,k} = \bar{Q}_{R_k, \Psi_{t,k}}$ be a uniform quantizer with the quantization interval $[-\Psi_{t,k}, \Psi_{t,k}]$ defined from

$$\Psi_{t,k} = \sum_{\tau=0}^{t} \sum_{k: t-\tau > T_k} \ell_{t-\tau,k+1} \tag{91}$$

We consider the control policy

$$u(t) = Q_{t,k}\left(\sum_{\tau=0}^{t} \sum_{k: t-\tau > T_k} e(t, k|\tau) \right). \tag{92}$$

Let us define the the quantization error $x_q(t)$ to be the sum of the errors from all quantizers $Q_{t,k}, k = \{1, 2, \cdots, m\}$, and the remaining errors in $x(t)$ to be the delay error $x_d(t)$. Observe that the delay error and the quantization error can be computed as follows:

$$x_d(t+1) = a^{T_k} w(t - T_k) + a^{T_k - 1} w(t - T_k + 1) + \cdots + w(t) \tag{93}$$

$$x_q(t+1) = u(t) - \sum_{\tau=0}^{t} \sum_{k: t-\tau > T_k} e(t, k|\tau) \tag{94}$$

Moreover, it can be shown that they are respectively bounded by

$$\mathbb{E}[x_d(t+1)] \le \sum_{h=1}^{T_1} |a^{h-1}|/2^{\mathcal{R}(h)} \tag{95}$$

$$\mathbb{E}[x_q(t+1)] \le \sum_{h=T_1+1}^{\infty} |a^{h-1}|/2^{\mathcal{R}(h)} \tag{96}$$

Therefore, the control policy Eq. 92 achieves the equality of Eq. 85.

F. Layered systems. We consider the layered system with two feedback loops

$$\begin{aligned}
x(t+1) &= ax(t) + u(t) + w(t) + r(t - T_a) \\
u(t) &= u_L(t) + u_H(t) \\
u_L(t) &= \mathcal{L}(x(0:t), w(0:t-1)) \\
u_H(t) &= \mathcal{H}(x(0:t), r(0:t-1))),
\end{aligned} \tag{97}$$

The disturbance is now composed of two terms: a component $r(t - T_a)$ that is observed with advance warning $T_a \ge 0$ and a component $w(t)$ that can be observed only through its impact on system performance. We assume that the two disturbances are bounded by

$$\|r\|_\infty \le 1, \quad \|w\|_\infty \le \delta. \tag{98}$$

The control action is generated by two nominally independent feedback loops, each having their own sensing, computation, and communication components. Both feedback loops, $\mathcal{L}, \mathcal{H}$ act through a motor nerve pathway with data rates R_L, R_H and delays T_L, T_H, respectively. The optimal cost in worst-case ℓ_∞ norm of this problem is

$$\inf_{\mathcal{H}, \mathcal{L}} \sup_{\|w\|_\infty \le \delta, \|r\|_\infty \le 1} \|x\|_\infty = \left\{ \sum_{i=0}^{T_L} |a^i| + \frac{|a^{T_L+1}|}{2^{R_L} - |a|} \right\} \delta + \frac{1}{2^{R_H} - |a|}. \tag{99}$$

To show Eq. 99, we first decompose Eq. 97 into

$$\begin{aligned} x_L(t+1) &= ax_L(t) + u_L(t) + w(t), \quad x_L(0) = 0 \\ u_L(t) &= \mathcal{L}(x(0:t), w(0:t-1)) \end{aligned} \tag{100}$$

and

$$\begin{aligned} x_H(t+1) &= ax_H(t) + u_H(t) + r(t-T_a), \quad x_H(0) = 0 \\ u_H(t) &= \mathcal{H}(x(0:t), r(0:t-1)). \end{aligned} \tag{101}$$

From linearity, we have

$$x(t) = x_L(t) + x_H(t). \tag{102}$$

Because the disturbances that steer the dynamics of $x_L(t)$ and $x_H(t)$ are disjoint, the optimal cost can also be decomposed into

$$\inf_{\mathcal{L},\mathcal{H}} \sup_{\|w\|_\infty \le 1} \|x\|_\infty = \inf_{\mathcal{L}} \sup_{\|w\|_\infty \le 1} \|x_L\|_\infty + \inf_{\mathcal{H}} \sup_{\|w\|_\infty \le 1} \|x_H\|_\infty \tag{103}$$

$$= \left\{ \sum_{i=0}^{T_L} |a^i| + \frac{|a^{T_L+1}|}{2^{R_L} - |a|} \right\} \delta + \frac{1}{2^{R_H} - |a|}, \tag{104}$$

which yields Eq. 99. In the last equality, we applied the results from section D on both sub-systems Eq. 100 and Eq. 101.

2. Stochastic setting with average-case performance

We consider the system with delayed and quantized control:

$$\begin{aligned} x(t+1) &= ax(t) + w(t-T_a) + u(t) \\ u(t+T_u) &= \mathcal{K}(x(0:t), w(0:t-1), u(0:t+T_u-1)) \end{aligned} \tag{105}$$

where $x(t) \in \mathbb{R}$ is the error, $u(t) \in \mathbb{R}$ is the control action, and $w(t) \in \mathbb{R}$ is the disturbance. The signal $w(t)$ is independent and identically distributed Gaussian random variables with zero mean and unit variance. The communication in the feedback loop is done through an arbitrary discrete-time channel that satisfies the following constraint:

$$\lim_{n\to\infty} \frac{1}{n} I(\{x(0:n), w(0:n-1)\}; u(0:n+T_u)) \le R \tag{106}$$

On special case of Eq. 106 is to have a quantizer of rate R in the feedback loop. The sensorimotor control in risk-neutral setting motivates the use of LQ control, and as such, our goal is to solve the following robust control problem:

$$\inf_{\mathcal{K}} \lim_{T\to\infty} \mathbb{E}\left[\frac{1}{T} \sum_{t=1}^{T} x(t)^2 \right] \tag{107}$$

subject to Eq. 105 and Eq. 106. This problem also admits a closed-form expression, a generalization of Eq. 6 in the main text, similar to its deterministic counterpart:

$$\lim_{T\to\infty} \mathbb{E}\left[\frac{1}{T} \sum_{t=1}^{T} x(t)^2 \right] \ge \sum_{i=0}^{T} |a^{2i}| + |a^{2(T+1)}| \left(2^{2R} - a^2\right)^{-1}, \tag{108}$$

where the equality is attained by an additive Gaussian channel with capacity R. In the special case when the channel is a quantizer with rate R, the right hand side of Eq. 108 is a lower-bound of the left hand side.

To show Eq. 108, recall from Section D that the error $x(t)$ can be decomposed into the term due to delayed control $x_d(t)$ and the term due to quantized control $x_q(t)$ as follows:

$$x(t) = x_d(t) + x_q(t). \tag{109}$$

Since both of them has zero mean and are independent from each other, the total cost can be decomposed into

$$\mathbb{E}[x(t)^2] = \mathbb{E}[x_d(t)^2 + x_q(t)^2]. \tag{110}$$

Since $x_d(t)$ is not a function of the control/communication policy, we have

$$\inf_{\mathcal{K}} \mathbb{E}[x(t)^2] = \mathbb{E}[x_d(t)^2] + \inf_{\mathcal{K}} \mathbb{E}[x_q(t)^2] \tag{111}$$

The first term satisfies

$$\mathbb{E}[x_d(t)^2] = \sum_{i=0}^{T} |a^{2i}|. \tag{112}$$

From (39, 50), the second term satisfies

$$\inf_{\mathcal{K}} \mathbb{E}[x_q(t)^2] = |a^{2(T+1)}| \left(2^{2a} - a^2\right)^{-1}. \tag{113}$$

where the equality is attained by an additive Gaussian channel with capacity R. Substituting Eq. 112 and Eq. 113 into Eq. 111, we obtain Eq. 6 in the main text.

3. Nerve signaling SATs

A. Spike-based encoding. In this section, we characterize the SATs for neural signaling in spike-based encoding and rate-based encoding. The result for spike-based encoding is also presented in our companion paper (28). In a spike-based encoding scheme, information is encoded in the presence or absence of a spike in specific time intervals, analogous to digital packet-switching networks (14, 15). We model the complex size distribution of axon bundles as being made up of m different groups of axons, indexed by $k \in \{1, 2, \cdots, m\}$, where each group contains axons with identical size. For each group k, we use n_k, ρ_k to denote the number of axons and their radius in that group. We use T_k, R_k to denote the delay and data rate (*i.e.* the amount of information in bits that can be transmitted) by group k, respectively. When the signaling is precise and noiseless, an axon with achievable firing rate ϕ can transmit ϕ bits of information per unit time. For sufficiently large myelinated axons, we assume that the propagation speed $1/T_k$ is proportional to the axon radius ρ_k (1), *i.e.*

$$T_k = \alpha/\rho_k \tag{114}$$

for some proportionality constant α. We also model the achievable firing rate ϕ_k of an axon in group k to be proportional to the axon radius ρ_k, *i.e.*

$$\phi_k = \beta\rho_k, \tag{115}$$

for some proportionality constant β. Moreover, the space and metabolic costs of a nerve are proportional to its volume (1), and given a fixed nerve length, these costs are proportional to its total cross-sectional area s_k. Combining above, we have

$$R_k = \lambda_k T_k, \qquad \sum_{k=1}^{m} \lambda_k = \frac{s\beta}{\pi\alpha}. \tag{116}$$

A special case of Eq. 116 is when all axons are uniform, *i.e.* when ρ_k are identical for all group k. For this case, Eq. 116 simplifies to

$$R = \sum_{k=1}^{n} \phi = \frac{s}{\pi\rho^2}\beta\rho = \frac{s\beta}{\pi}\frac{1}{\rho} = \frac{s\beta}{\alpha\pi}T_s. \tag{117}$$

This leads to $R = \lambda T_s$, where $\lambda = s\beta/\pi\alpha$ is proportional to the spatial and metabolic cost to build and maintain the nerves. When the signaling is precise and noiseless, the amount of information per unit time (bits/sec) that an axon with achievable firing rate ϕ can transmit is simply:

$$C_s = \phi. \tag{118}$$

B. Rate-based encoding. In a rate-based encoding scheme, information is encoded in the spike rate. We can think of the rate-based encoding as a Poisson-type communication channel whose input is the spike rate $\gamma(t)$ and the output is the spike timing $M(t)$. We assume that the spike timing is a non-homogeneous Poisson point process with rate (intensity) $\gamma = \{\gamma(t) \geq 0 : t \in \mathbb{R}_+\}$, denoted by $\mathcal{P}_t(\gamma)$. The communication channel is then given by

$$M(t) = \mathcal{P}_t(\gamma). \tag{119}$$

where the spike rate is bounded by

$$\gamma(t) \leq \phi \qquad t \in \mathbb{R}_+, \tag{120}$$

for some $\phi > 0$. The capacity of communication channel Eq. 119 is defined to be

$$C_r = \sup \lim_{T\to\infty} \frac{1}{T} I(\gamma^T; M^T), \tag{121}$$

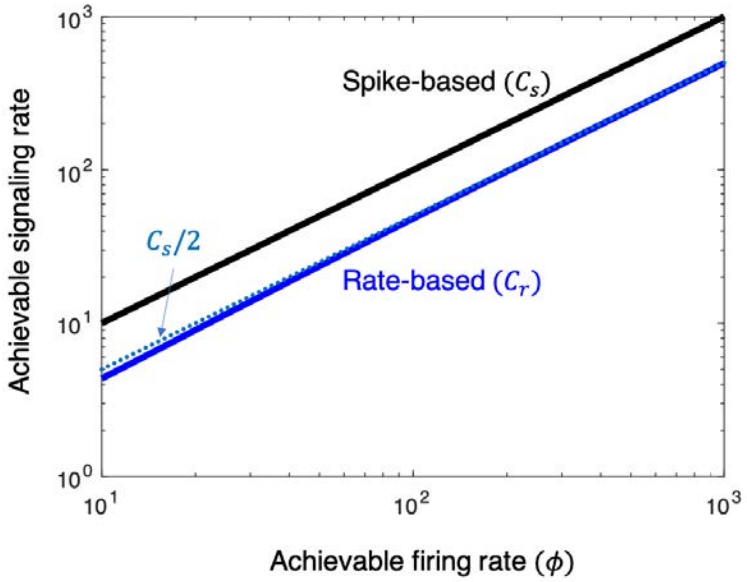

Fig. 8. The signaling rate in spike-based coding vs. rate-based coding given a fixed resource to build and maintain nerves. The solid black line shows the achievable signaling rate C_s from Eq. 118 in spike-based coding; the solid blue line shows the achievable signaling rate C_r from Eq. 122 in rate-based coding; and the dotted blue line shows $C_s/2$. The rate of the rate-based encoding is less than half of that of spike-based encoding and approaches to half of the spike-based encoding rate as the achievable firing rate increases (see Eq. 123). This suggests that spike-based encoding may transmit more information, particularly when the achievable firing rate ϕ is small.

where the supremum is taken over all distributions of the input process $\mathcal{P}_{\gamma(t)}$ satisfying Eq. 120. Kabanov has shown in (51) that C_r is upper-bounded by

$$C_r = \frac{(\phi+1)^{1+\phi^{-1}}}{2} - \left(1+\frac{1}{\phi}\right)\log(\phi+1). \quad [122]$$

So for sufficiently large ϕ, we have

$$C_r \to \phi/2 \text{ as } \phi \to \infty, \quad [123]$$

which yields Eq. 13 in the main text.

4. Additional experimental results

We tested how the hardware SATs constrain the SATs in driving. Specifically, we studied three settings: driving with added delay, added quantization, and both. We quantified the system performance using the mean squared error between the actual trajectory and the desired one. We generated the turning angle (alternating to left or right) of the trail from the uniform distribution with domain $[10, 45]$. In the setting of added delay, we set the delay to be $-4, -3, ..., 2$ sampling intervals, respectively, where each sampling interval is 16.67 ms. In the setting of added quantization, we set the rates of the quantizer to be $1, 2, ..., 7$ bits per unit sampling interval. In the case of added delay and quantization, we let the delay and rate to satisfy the relation $T = (R-5)/15$. Each set of parameter was tested for 30 seconds before switching to others. The experimental results are compared with the theoretical prediction in Fig. 9.

1. P. Sterling, S. Laughlin, *Principles of neural design* (MIT Press, 2015).
2. J. A. Perge, K. Koch, R. Miller, P. Sterling, V. Balasubramanian, *Journal of Neuroscience* **29**, 7917 (2009).
3. J. A. Perge, J. E. Niven, E. Mugnaini, V. Balasubramanian, P. Sterling, *Journal of Neuroscience* **32**, 626 (2012).
4. L. Zhaoping, *Understanding vision: theory, models, and data* (Oxford University Press, 2014).
5. P. M. Fitts, J. R. Peterson, *Journal of experimental psychology* **67**, 103 (1964).
6. A. J. Nagengast, D. A. Braun, D. M. Wolpert, *Journal of neurophysiology* **105**, 2668 (2011).
7. R. J. van Beers, P. Baraduc, D. M. Wolpert, *Phil. Trans. of the Royal Society B: Bio. Sciences* **357**, 1137 (2002).
8. E. Todorov, M. I. Jordan, *Nature neuroscience* **5**, 1226 (2002).
9. K. Padmanabhan, N. N. Urban, *Nature neuroscience* **13**, 1276 (2010).
10. S. Lac, J. L. Raymond, T. J. Sejnowski, S. G. Lisberger, *Annual review of neuroscience* **18**, 409 (1995).
11. S. G. Lisberger, *Neuron* **66**, 477 (2010).
12. J. Massion, *Progress in neurobiology* **38**, 35 (1992).
13. S. Bouisset, M.-C. Do, *Neurophysiologie Clinique/Clinical Neurophysiology* **38**, 345 (2008).
14. E. Salinas, T. J. Sejnowski, *Nature reviews neuroscience* **2**, 539 (2001).
15. K. H. Srivastava, *et al.*, *Proceedings of the National Academy of Sciences* **114**, 1171 (2017).
16. Z. F. Mainen, T. J. Sejnowski, *Science* **268**, 1503 (1995).
17. J. L. Fox, A. L. Fairhall, T. L. Daniel, *Proceedings of the National Academy of Sciences* p. 200912548 (2010).
18. P. Whittle (1990).

A

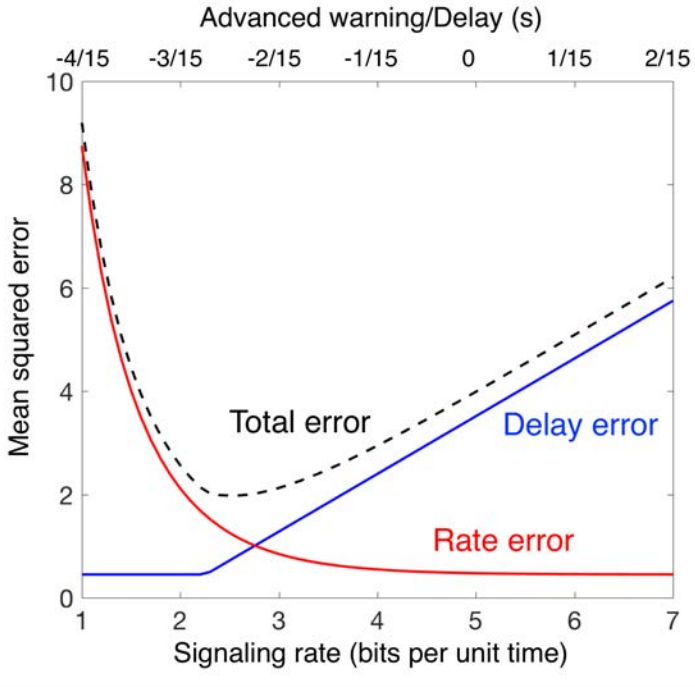

B

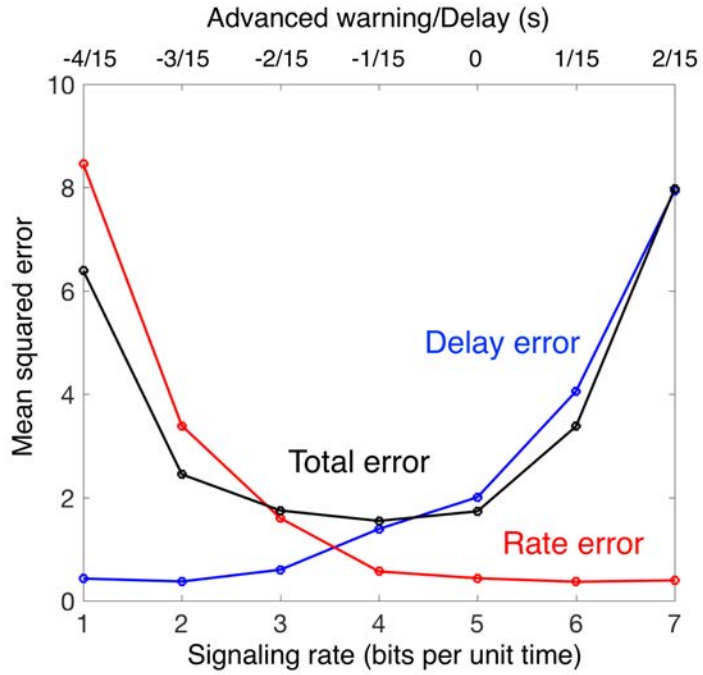

Fig. 9. Theoretical and experimental system SATs in sensorimotor control (average-case). *(A)* Theoretical SATs in the tracking (driving) task. The delay error (blue), rate error (red), and the total error (black) in Eq. 6 are shown with varying hardware SAT $T = (R - 5)/15$. *(B)* Empirical SATs in the tracking (driving) task. The error under added delay (blue), the error under added quantization (red); and the error under added delayed and quantization (black) are shown. In the last case, the added delay T and quantization rate R satisfy $T = (R - 5)/15$. The shadowed area indicates the standard error across subjects.

19. H. Nagai, *SIAM journal on control and optimization* **34**, 74 (1996).
20. T. D. Sanger, *Engineering in Medicine and Biology Society (EMBC), 2010 Annual International Conference of the IEEE* (IEEE, 2010), pp. 4494–4497.
21. T. D. Sanger, *Neural computation* **26**, 2669 (2014).
22. Y. P. Leong, J. C. Doyle, *Decision and Control (CDC), 2016 IEEE 55th Conference on* (IEEE, 2016), pp. 1508–1514.
23. C. Bodelon, M. Fallah, J. H. Reynolds, *Journal of Vision* **5**, 758 (2005).
24. C. Koch, N. Tsuchiya, *Trends in cognitive sciences* **11**, 16 (2007).
25. P. E. Roland, *et al.*, *Proceedings of the National Academy of Sciences* **103**, 12586 (2006).
26. P. B. Matthews, *Trends in neurosciences* **14**, 87 (1991).
27. D. Kahneman, P. Egan, *Thinking, fast and slow*, vol. 1 (Farrar, Straus and Giroux New York, 2011).
28. Y. Nakahira, Q. Liu, T. Sejnowski, J. C. Doyle, *https://arxiv.org/submit/2714509* (2019).
29. D. Beamish, S. A. Bhatti, I. S. MacKenzie, J. Wu, *Journal of The Royal Society Interface* **3**, 649 (2006).
30. L. Muckli, L. S. Petro, *Current opinion in neurobiology* **23**, 195 (2013).
31. R. P. Heitz, *Frontiers in neuroscience* **8**, 150 (2014).
32. A. K. Abbas, A. H. Lichtman, S. Pillai, *Basic Immunology E-Book: Functions and Disorders of the Immune System* (Elsevier Health Sciences, 2015).
33. L. M. Sompayrac, *How the immune system works* (Wiley-Blackwell, 2019).
34. A. Ehsan, Q. Yang, *Applied energy* **210**, 44 (2018).
35. P. Kundur, N. J. Balu, M. G. Lauby, *Power system stability and control*, vol. 7 (McGraw-hill New York, 1994).
36. A. D. JoSEP, *et al.*, *Communications of the ACM* **53** (2010).
37. W. Shi, J. Cao, Q. Zhang, Y. Li, L. Xu, *IEEE Internet of Things Journal* **3**, 637 (2016).
38. R. G. R. Stein, K. Jones, *Nature Reviews Neuroscience* **6**, 389 (2005).
39. S. Tatikonda, A. Sahai, S. Mitter, *IEEE transactions on Automatic Control* **49**, 1549 (2004).
40. T. Tanaka, P. M. Esfahani, S. K. Mitter, *IEEE Transactions on Automatic Control* **63**, 37 (2018).
41. V. Kostina, B. Hassibi (IEEE, 2019).
42. Y. Nakahira, F. Xiao, V. Kostina, J. C. Doyle, *2018 Annual American Control Conference (ACC)* (IEEE, 2018), pp. 2707–2714.
43. Q. Liu, Y. Nakahira, A. Mohideen, S. Choi, J. C. Doyle, Wheelcon: A wheel control-based gaming platform for studying human sensorimotor control (2018). Https://arxiv.org/abs/1811.00738.
44. J. C. Doyle, B. A. Francis, A. R. Tannenbaum, *Feedback control theory* (Courier Corporation, 2013).
45. M. A. Dahleh, I. J. Diaz-Bobillo, *Control of Uncertain Systems: A Linear Programming Approach* (Prentice-Hall, Inc., Upper Saddle River, NJ, USA, 1995).
46. S. Tatikonda, S. Mitter, *IEEE Transactions on Automatic Control* **49**, 1056 (2004).
47. P. K. H. Ouden, F. Lange, *Frontiers is Psychology* (2012).
48. G. N. Nair, F. Fagnani, S. Zampieri, R. J. Evans, *Proceedings of the IEEE* **95**, 108 (2007).
49. Y.-S. Wang, N. Matni, J. C. Doyle, *arXiv preprint arXiv:1610.04815* (2016).
50. A. Gorbunov, M. S. Pinsker, *Problemy Peredachi Informatsii* **10**, 5 (1974).
51. H. A. M. Davis, *IEEE Transactions on Information Theory* **26**, 710 (1980).